Inorganic Chemistry

Article

pubs.acs.org/IC

$Ca_{12}InC_{13-x}$ and $Ba_{12}InC_{18}H_4$: Alkaline-Earth Indium Allenylides Synthesized in AE/Li Flux (AE = Ca, Ba)

Trevor V. Blankenship, Matthew J. Dickman, Lambertus J. van de Burgt, and Susan E. Latturner*

Department of Chemistry and Biochemistry, Florida State University, Tallahassee, Florida 32306, United States

Supporting Information

ABSTRACT: Two new complex main-group metal carbides were synthesized from reactions of indium, carbon, and a metal hydride in metal flux mixtures of an alkaline earth (AE = Ca, Ba) and lithium. $Ca_{12}InC_{13-x}$ and $Ba_{12}InC_{18}H_4$ both crystallize in cubic space group $Im\bar{3}$ [a = 9.6055(8) and 11.1447(7) Å, respectively]. Their related structures are both built on a body-centered-cubic array of icosahedral clusters comprised of an indium atom and 12 surrounding alkaline-earth cations; these clusters are connected by bridging monatomic anions (either H^- or C^{4-}) and allenylide anions, C_3^{4-}. The allenylide anions were characterized by Raman spectroscopy and hydrolysis studies. Density of states and crystal orbital Hamilton population calculations confirm that both compounds are metallic.

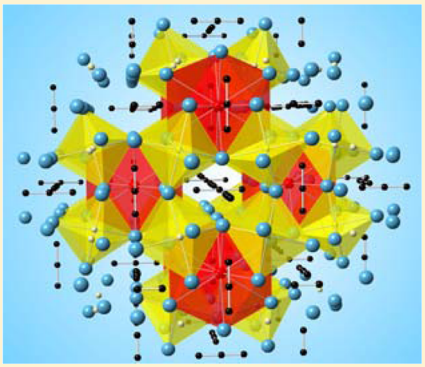

INTRODUCTION

Reactions of electropositive elements from groups 1 and 2 with main-group p-block metals and metalloids often result in electron transfer and the formation of charge-balanced Zintl phases. Depending on the reactant ratio, the p-block elements accept electrons and/or form M−M bonds to fill their valence shells.[1] For instance, tin can exist in Zintl phases as isolated Sn^{4-} anions (in $Ca_{11}Sn_3C_8$), clusters such as Sn_4^{4-} (in Na_4Sn_4) and Sn_9^{4-} (K_4Sn_9), or anionic layers or networks as in K_8Sn_{44}.[2,3] However, a "Zintl border" exists between groups 13 and 14; group 13 metals are typically not electronegative enough to form Zintl anions. Elements such as gallium and indium therefore exhibit a rich and unpredictable chemistry. The Corbett group explored this extensively, discovering binary and ternary polar-but-not-charge-balanced intermetallic phases of indium with alkali and alkaline-earth metals that feature unusual clusters such as the In_{11}^{7-} cluster in K_8In_{11}, the linked In_{12}, In_{15}, and In_{16} species in $K_{39}In_{80}$, and the In_{28} species in $K_{34}In_{92.3}Li_{12.7}$, $K_{14}Na_{20}In_{91.82}Li_{13.8}$, and $K_{14}Na_{20}In_{96}$.[4−6]

In the process of exploring reactions of alkaline-earth metals with group 13 and 14 elements, the Corbett group also investigated inadvertent hydride incorporation. Closer examination of reported phases such as Ba_5Ga_6 and $Ba_{21}Ge_2O_5$ indicated that they were actually hydrides ($Ba_5Ga_6H_2$ and $Ba_{21}Ge_2O_5H_{24}$, respectively); their formation was facilitated by the use of hydrogen-contaminated barium.[7,8] Alkaline-earth metals react with trace water vapor to form hydrogen; this diffuses readily into the bulk metal to form a solid solution. As a result, commercially available heavier alkaline earths (Ca, Sr, and Ba) may contain 5−20 atomic % hydrogen, with barium being the most susceptible to a high level of contamination.

We are deliberately using the high solubility of hydrogen, carbon, and other light elements in alkaline-earth metal-rich fluxes to synthesize complex intermetallic hydrides and carbides. Metal flux synthesis involves the use of an excess of low-melting metal as a reaction medium. Upon melting, this metal acts as a solvent for other reactants present, bringing them into solution to react with each other (and potentially with the flux metal itself) to form products.[9] Alkaline-earth metals are higher melting than the more commonly used metal fluxes (such as Sn, In, Ga, and Al); however, the melting point is lowered upon the addition of lithium. A 50:50 mol% mixture of Ca/Li melts at around 300 °C, as does a similar Ba/Li mixture.[10] Main-group elements are highly soluble in alkaline earth/lithium mixtures. (Ca/Li)/M/CaH_2 reactions with M = group 14 or 15 elements have produced charge-balanced Zintl phase hydrides such as $LiCa_2C_3H$, $LiCa_7Ge_3H_3$, and $LiCa_3As_2H$.[11−13] Our initial investigations into similar reactions with group 13 metals such as indium led to a very unusual "subhydride" compound, $Ca_{54}In_{13}B_4H_{23}$, which contains ionic hydride regions and metallic Ca/In regions.[14] Further reactions of indium with other elements in AE/Li fluxes have led to two new phases, $Ca_{12}InC_{13-x}$ and $Ba_{12}InC_{18}H_4$. Both of these phases contain indium atoms coordinated by 12 alkaline-earth cations; these clusters are packed in a body-centered-cubic (bcc) array and linked by either H^- or C^{4-} anions. The remaining void spaces are filled by C_3^{4-} allenylide anions, which were observable by Raman spectroscopy and mass spectrometric studies of hydrolysis products. Density of states (DOS) and crystal orbital Hamilton population (COHP) calculations confirm the metallic nature of these phases.

Special Issue: To Honor the Memory of Prof. John D. Corbett

Received: September 23, 2014
Published: November 6, 2014

   dx.doi.org/10.1021/ic502315m | Inorg. Chem. 2015, 54, 914−921

EXPERIMENTAL PROCEDURE

Synthesis. $Ba_{12}InC_{18}H_4$ was synthesized from reactions of indium, LiH, and carbon in Ba/Li flux. Chunks of lithium (99.8% Strem), barium (99%, Alfa Aesar), acetylene carbon black powder (99.5% Alfa Aesar), indium powder (99.9%, Alfa Aesar), and lithium hydride powder (97%, Alfa Aesar) were used as received. Reactants and flux metals were added to stainless steel crucibles (7.0 cm length and 0.7 cm diameter) in a 8:8:0.8:0.8:0.8 mmol Ba/Li/In/C/LiH ratio in an argon-filled glovebox. The crucibles were sealed by arc-welding under argon and placed in silica tubes, which were flame-sealed under vacuum. The ampules were heated from room temperature to 1050 °C in 3 h and held there for 2 h. The reactions were cooled stepwise to 800 °C in 72 h and 500 °C in 36 h and then held at 500 °C for 24 h. The reactions were then removed from the furnace, inverted, and centrifuged for 2 min to separate the crystalline products from the Ca/Li melt. The solid product adheres to the side of the crucible. The steel crucibles were cut open in an argon-filled glovebox.

$Ca_{12}InC_{13-x}$ was initially found as a product of reactions of indium and carbon in Ca/Li flux, which used the calcium metal as received (99.5%, Alfa Aesar), without subsequent purification to remove hydride contamination. The reactants Ca/Li/In/C were combined in a 7:7:1:2 mmol ratio and placed in a stainless steel crucible. This was arc-welded shut under argon and then placed into a silica tube, which was flame-sealed under vacuum. The ampule was heated using the same heating profile as the $Ba_{12}InC_{18}H_4$ synthesis. After crystallographic studies (see below), further syntheses were carried out to determine the likely occupancy of a possible mixed C/H site. Syntheses using added CaH_2 were explored, with reactions such as Ca/Li/In/C/CaH_2 producing $Ca_{54}In_{13}H_{27}$ (a boron-free variant of $Ca_{54}In_{13}B_{4-x}H_{23+x}$ in $Im\bar{3}$, a = 16.28 Å)[14] instead of the desired carbide phase. Subsequent syntheses were carried out without any hydride added and using calcium that was purified by heating to 700 °C under high vacuum to remove any hydride contaminants. These Ca/Li/In/C reactions yielded the desired phase, supporting its identification as a carbide ($Ca_{12}InC_{13-x}$) and not a carbide hydride ($Ca_{12}InC_{9+x}H_{4-x}$). The optimized Ca/Li/In/C reactant ratio of 7:7:1:3 was combined and heated as described above.

Elemental Analysis. Elemental analyses were performed using scanning electron microscopy (SEM; JEOL 5900) with energy-dispersive spectroscopy (EDS) capabilities. Samples of product crystals were affixed to an aluminum SEM stub using carbon tape and analyzed using a 30 kV accelerating voltage. The EDS detector is not sensitive to the presence of light elements such as carbon and hydrogen, so only the relative ratios of alkaline earth and indium were observed. The observed AE/In atomic ratios averaged 90:10 for both $Ca_{12}InC_{13-x}$ and $Ba_{12}InC_{18}H_4$. No incorporation of metals from the steel crucible (Fe, Ni, and Mo) was detected in any of the samples.

Crystallographic Analysis. Samples of $Ca_{12}InC_{13-x}$ and $Ba_{12}InC_{18}H_4$ were brought out of the glovebox under Paratone oil and examined under a microscope to select crystals for diffraction studies. Spheroid crystals of suitable size were mounted in cryoloops. Single-crystal X-ray diffraction data were collected at 200 K under a stream of nitrogen using a Bruker APEX 2 CCD diffractometer with a Mo Kα radiation source. Absorption corrections were applied to the data sets using the *SADABS* program.[15] Refinements of the structures were performed using the *SHELXTL* package.[16] The structure solutions for both compounds were complicated by possible lower-symmetry cells (with the software recommending a rhombohedral setting for the calcium phase and a monoclinic setting for the barium phase), but the apparent cubic metrics of the unit cell parameters enabled selection of the proper cell symmetry. The structure of $Ba_{12}InC_{18}H_4$ was initially solved in cubic space group $I23$, but use of the *AddSym* program in the *PLATON* software suite indicated the presence of additional symmetry elements and converted the structure to space group $Im\bar{3}$ (No. 204).[17] It was subsequently found that the $Ca_{12}InC_{13-x}$ structure could also be solved in this space group. For both structures, alkaline-earth and indium sites were determined using direct methods. Light element positions were located using difference Fourier calculations. Refinement of the allenylide carbon sites was straightforward, with occupancies refining at/near 100% and bond lengths confirming their identity as carbon atoms in a C_3^{4-} unit. The 8c sites presented the most difficulty in both structures, being occupied by a light atom octahedrally coordinated by surrounding heavy alkaline-earth cations. These sites were initially assigned as carbon, with partial occupancy indicated in both phases; if assigned as hydrogen, both refinements indicated greater than 100% occupancy (slightly above 100% for the barium phase; well over 100% for the calcium phase). This could be due to the fact that this site is occupied by a hydride anion (with two electrons instead of one), by a mixture of H^- and C^{4-}, or by partially occupied C^{4-}. The barium phase refinement proved to be stable with this site assigned as a fully occupied hydride, leading to the stoichiometry $Ba_{12}InC_{18}H_4$. For the calcium compound, refining this site as a hydride site led to very high and unstable occupancy, negative thermal parameters, and much higher R values. This site could instead be refined as partially occupied by carbon (at 68%, as shown in Tables 1 and 2) or as fully occupied by

Table 1. Crystallographic Data Collection Parameters for the Title Phases

	$Ca_{12}InC_{11.7}$	$Ba_{12}InC_{18}H_4$
fw	736.30	1983.11
cryst syst	cubic	cubic
space group	$Im\bar{3}$ (No. 204)	$Im\bar{3}$ (No. 204)
a (Å)	9.6055(8)	11.1447(7)
Z	2	2
volume (Å^3)	886.3(1)	1384.2(1)
density, calcd (g cm^{-3})	2.759	4.758
Index ranges	$-12 \le h \le 12$, $-12 \le k \le 12$, $-12 \le l \le 12$	$-14 \le h \le 14$, $-14 \le k \le 14$, $-14 \le l \le 14$
temperature (K)	200	200
reflns collected	4634	7912
unique data/param	223/19	331/21
μ (mm^{-1})	4.79	17.57
R1/wR2[a]	0.0199/00382	0.0178/0.0447
R1/wR2 (all data)	0.0260/0.0397	0.0178/0.0447
residual peak/hole (e$^-$ A^{-3})	0.37/−0.66	0.62/−1.86

[a] $R1 = \sum||F_o| - |F_c||/\sum|F_o|$; $wR2 = [\sum[w(F_o^2 - F_c^2)^2]/\sum[w(F_o^2)^2]]^{1/2}$.

Table 2. Atomic Coordinates and Isotropic Thermal Parameters for the Title Phases

atom	Wyckoff site	x	y	z	U_{eq}[a]
			$Ba_{12}InC_{18}H_4$		
In1	2a	0	0	0	0.0209(3)
Ba1	24g	0.30273(3)	0.18009(3)	0	0.0168(2)
C1	12e	0.1517(10)	$^1/_2$	0	0.040(2)
C2	24g	0.1606(6)	0.3815(7)	0	0.030(1)
H1	8c	$^1/_4$	$^1/_4$	$^1/_4$	0.03(3)
			$Ca_{12}InC_{13-x}$		
In1	2a	0	0	0	0.0090(2)
Ca1	24g	0.30553(6)	0.18892(6)	0	0.0159(2)
C1	6b	$^1/_2$	0	0	0.012(1)
C2	12e	$^1/_2$	0	0.1357(4)	0.026(1)
C3[b]	8c	$^1/_4$	$^1/_4$	$^1/_4$	0.018(2)

[a] U_{eq} is defined as one-third of the trace of the orthogonalized U_{ij} tensor. [b] All sites are fully occupied with the exception of the C3 site of $Ca_{12}InC_{11.7}$ [68(1)% occupied].

dx.doi.org/10.1021/ic502315m | Inorg. Chem. 2015, 54, 914−921

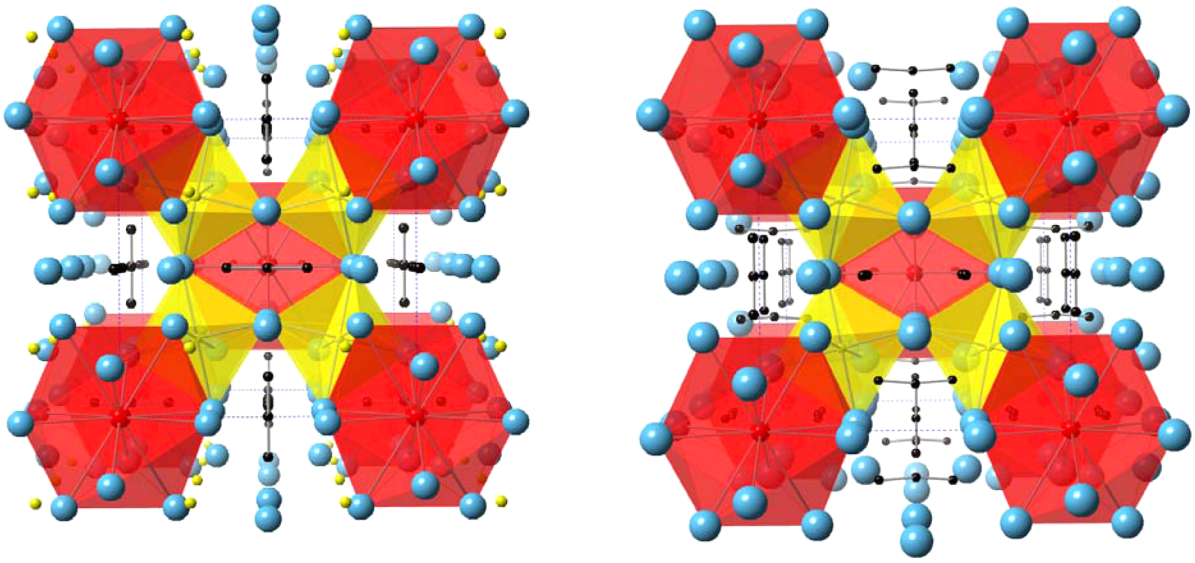

Figure 1. Cubic structures of $Ca_{12}InC_{13-x}$ (left) and $Ba_{12}InC_{18}H_4$ (right). Alkaline-earth atoms are blue, and allenylide carbon atoms are black; the local coordination environments of C^{4-}/H^- and indium atoms are highlighted as yellow and red polyhedra, respectively.

a mixture of carbon and hydrogen (at 61% and 39% occupancy, respectively; see Tables S1 and S2 in the Supporting Information, SI). The refinement parameters of the $Ca_{12}InC_{11.7}$ and $Ca_{12}InC_{11.5}H_{1.5}$ models are almost identical. The $Ca_{12}InC_{11.7}$ model (with the partially occupied carbide site) was chosen after rigorously hydride-free syntheses were carried out, which successfully yielded the target product. Several data sets were collected on crystals from different synthesis batches, with the carbon occupancy on this site averaging 71(3)% (for a stoichiometry of $Ca_{12}InC_{11.8}$). Crystallographic data collection and refinement parameters for $Ba_{12}InC_{18}H_4$ and $Ca_{12}InC_{11.7}$ are shown in Table 1, and atomic positions are listed in Table 2; additional refinement models and CIF files are found in the SI.

Electronic Structure Calculations. DOS and COHP calculations for both title compounds were carried out using the Stuttgart *TB-LMTO-ASA* software package, based on the unit cell dimensions and atomic coordinates derived from single-crystal diffraction data.[18] For $Ca_{12}InC_{13-x}$, an ordered model compound with the carbide 8c site fully occupied was used ($Ca_{12}InC_{13}$). Empty spheres were added by the program where appropriate to fill the unit cell volume. A 12 × 12 × 12 *k*-point mesh was used and integrated using the tetrahedron method. The basis sets for $Ba_{12}InC_{18}H_4$ consisted of In 5s/5p, Ba 6s/5d/4f, C 2s/2p, and H 1s orbitals. The In 5d/4f, Ba 6p, C 3d, and H 2s/2p orbitals were downfolded. For $Ca_{12}InC_{13}$, the basis sets consisted of In 5s/5p, Ca 4s/3d, and C 2s/2p orbitals.

Raman Spectroscopy. Crystals of $Ca_{12}InC_{13-x}$ and $Ba_{12}InC_{18}H_4$ were sandwiched between quartz slides, which were sealed together with TorrSeal epoxy under argon. The Raman measurements were carried out using a JY Horiba LabRam HR800 system excited by a HeNe laser emitting at 633 nm. The spectrograph uses an edge filter to couple the laser beam into the microscope (Olympus BX30) by total reflection. The beam is focused on the sample through a microscope objective 50× IR (Leica NA 0.80). Scattered radiation is collected by the objective, and laser radiation is filtered out by the edge filter, with Raman scattering coupled into the spectrograph CCD through a confocal hole. Spectra were collected under ambient conditions over the spectral range of 100−3200 cm^{-1}.

Hydrolysis Studies. The $Ca_{12}InC_{13-x}$ and $Ba_{12}InC_{18}H_4$ samples were reacted with water to explore hydrolysis of the carbide anions in their structures. Crystals were placed in a 200 mL Schlenk flask sealed with a rubber septum under argon. The reaction with water occurs instantly at room temperature, forming gaseous products upon the addition of 5 μL of water. Aliquots of the product gases were taken by syringe and analyzed by injecting them into a HP 6890 series gas chromatograph system coupled to a HP 5973 mass-selective detector.

RESULTS AND DISCUSSION

Synthesis. $Ca_{12}InC_{13-x}$ crystallizes as small silver cubes up to 1 mm on a side. The yield is 70% based on carbon; byproducts include CaC_2 and an unidentified reddish phase in small quantities. The $Ba_{12}InC_{18}H_4$ phase forms as bronze nonfaceted chunks of about 0.5−1 mm size. Reactions averaged about a 30% yield based on carbon. BaC_2 and Ba_3FeN_3 are commonly seen as byproducts. The latter phase is probably due to nitrogen impurities in the lithium metal and iron that is leached from the crucible. Carbon is leached from the crucible as well to form the title phase; it was initially isolated in small amounts from a Ba/Li/In/LiH reaction without added carbon. The formation of BaC_2 makes it difficult to improve yields because adding more carbon pushes the reaction to favor BaC_2. Both $Ca_{12}InC_{13-x}$ and $Ba_{12}InC_{18}H_4$ are highly air-sensitive, reacting readily with air or water. Mass spectrometry on the products of hydrolysis indicates the formation of allene (C_3H_4) for both compounds; see Figure S1 in the SI. Traces of acetylene were also seen in the mass spectra of both phases due to hydrolysis of the AEC_2 byproducts.

Structure Description. Both title phases exhibit new crystal structures in space group $Im\bar{3}$ based on a bcc packing of indium-centered alkaline-earth icosahedra, $In@AE_{12}$, shown as red polyhedra in Figure 1. The indium atoms of both structures occupy a 2a site (in the corners and center of the unit cell) and are surrounded by 12 alkaline-earth cations, which occupy 24g sites. A similar bcc packing of $In@AE_{12}$ clusters is found in $Ca_{54}In_{13}B_{4-x}H_{23+x}$, also grown from Ca/Li flux; the $In@Ca_{12}$ clusters in that structure have a somewhat shorter In−Ca distance [3.3400(7) Å] compared to that in $Ca_{12}InC_{13-x}$ [3.4505(7) Å].[14] The binary phase Ca_8In_3 also features indium sites surrounded by calcium cations, exhibiting Ca−In distances in the 3.25−3.81 Å range.[19] Other calcium indide phases have more In−In bonding but feature similar Ca−In bond distances (ranging from 3.2 to 3.7 Å in $Ca_{18}Li_5In_{25}$ and Ca_2In).[20,21] The $In@Ba_{12}$ clusters in $Ba_{12}InC_{18}H_4$ can be compared to similar indium-centered clusters in Ba_9In_4H and $Ba_{21}In_2O_5H_x$.[22,8] While bond-length data for the distorted icosahedral $In@Ba_{12}$ units in the latter compound are not available, the $In@Ba_{10}$ units in Ba_9In_4H exhibit In−Ba distances ranging from 3.52 to

dx.doi.org/10.1021/ic502315m | *Inorg. Chem.* 2015, 54, 914−921

4.25 Å. The observed In−Ba distance in the close-to-ideal In@Ba_{12} icosahedra of $Ba_{12}InC_{18}H_4$ is in the middle of this range at 3.9259(4) Å (Table 3). It is also within the 3.53−4.19 Å range seen for the 11-coordinate indium sites found in $Ba_5Al_{4.1}In_{1.9}$.[23]

Table 3. Bond Lengths (Å) in the Title Phases, Where AE = Alkaline Earth (Ca or Ba)

bond	$Ca_{12}InC_{11.7}$	$Ba_{12}InC_{18}H_4$
In−AE	3.4505(7) (×12)	3.9257(4) (×12)
C1−C2	1.304(4) (×2)	1.325(7) (×2)
C1−AE	2.6043(6) (×4)	2.889(7) (×2), 3.423(5) (×4)
C2−AE	2.515(3) (×2), 2.912(2) (×4)	2.747(7) (×1), 2.829(5) (×2), 3.120(5) (×2)
8c site−AE	2.5289(3) (×6)	2.9521(2) (×6)

Eight of the triangular faces of the In@AE_{12} icosahedra are capped by light atom sites on 8c Wyckoff sites. This position is occupied by hydride ions in $Ba_{12}InC_{18}H_4$ and partially occupied by carbide ions in $Ca_{12}InC_{13-x}$. These sites bridge the icosahedral clusters, with three alkaline-earth cations from one cluster and three from a neighboring cluster forming an overall octahedral coordination around this site (shown as yellow polyhedra in Figure 1). In $Ba_{12}InC_{18}H_4$, the resulting H@Ba_6 units have a Ba−H distance of 2.952 Å, very similar to the 2.955 and 2.970 Å distances observed for the same building blocks in Ba_9In_4H.[22] It is also comparable to BaH_2, which has Ba−H bond lengths from 2.60 to 3.00 Å.[24] While bond valence sum (BVS) calculations are not typically used for metallic compounds, the hydride site is likely to be somewhat ionic, and it has a BVS of 0.83. This value indicates that the hydride is slightly underbonded, but the value is in the range seen for other phases containing H@Ba_6 units, including BaH_2, Ba_2H_3Cl, and Ba_2H_3Br.[25] Hydride anions are highly polarizible and are known to adapt their volume to a variety of coordination environments.[26]

The presence of carbide anions on the 8c site in $Ca_{12}InC_{13-x}$ was confirmed in synthetic experiments (this compound forms in the absence of hydride sources) and in the crystallographic data refinement. Full occupancy of this site would lead to a stoichiometry of $Ca_{12}InC_{13}$, but partial occupancy was indicated, with several data sets supporting a stoichiometry of $Ca_{12}InC_{13-x}$ ($x \approx 1.3$). The octahedral C^{4-}@Ca_6 units have a Ca−C distance of 2.5289(3) Å. It is notable that no calcium methanide exists with comparable monatomic C^{4-} anions. While the methanide Be_2C is the stable binary carbide for beryllium and a high-pressure magnesium methanide Mg_2C was recently reported, no methanides are known for the heavier alkaline earths; those MC_2 metal carbides (M = Ca, Sr, Ba) contain acetylide anions instead.[27,28] $Ca_{12}InC_{13-x}$ is also one of a select few metal carbides featuring two different types of carbide anion; monatomic C^{4-} and the triatomic allenylide anion C_3^{4-} (vide infra) are also found in Ln_4C_7 (Ln = Ho, Er, Tm, Lu), Sc_3C_4, and $R_5Re_2C_7$ (R = Er, Tm, Lu, Sc).[29−31]

The remainder of the space in the structures of $Ca_{12}InC_{13-x}$ and $Ba_{12}InC_{18}H_4$ is filled by allenylide anions, C_3^{4-}. Their identity as allenylides is confirmed by the fact that hydrolysis reactions of both phases produce allene gas (C_3H_4). In the solids, these C_3^{4-} species are nearly linear, with C−C bond lengths that clearly indicate double bonds [1.304(4) Å and linear in the calcium compound; 1.325(7) Å with a 171° angle in the barium phase). Very similar bond lengths (in the 1.30−1.33 Å range) are seen in charge-balanced allenylide salts such as Mg_2C_3, $Ca_3C_3Cl_2$, $LiCa_2C_3H$, and $Ca_{11}Sn_3C_8$, as well as in metallic carbides including Ln_4C_7, Sc_3C_4, and $R_5Re_2C_7$.[32,33,11,2,29−31] The packing of the C_3^{4-} anions is different in $Ca_{12}InC_{13-x}$ and $Ba_{12}InC_{18}H_4$, as shown in Figure 2. In both compounds, these linear anions are aligned parallel to the axes of the unit cell and positioned between the In@AE_{12} icosahedral clusters. The barium phase has larger voids between the In@Ba_{12} units, allowing for the incorporation of twice as many allenylide anions. In the calcium compound, the C_3^{4-} anions are surrounded by two face-sharing square antiprisms of calcium cations, one encapsulating each terminal carbon atom. The same arrangement of barium atoms (two face-sharing square antiprisms) can encapsulate two C_3^{4-} units, one enveloped in each square antiprism.

The Raman spectra of both phases, shown in Figure 3, are both dominated by the stretching modes of the allenylide anions. The spectrum of $Ca_{12}InC_{13-x}$ shows the symmetric and asymmetric stretching modes at ν_{sym} = 1100 cm^{-1} and ν_{asym} =

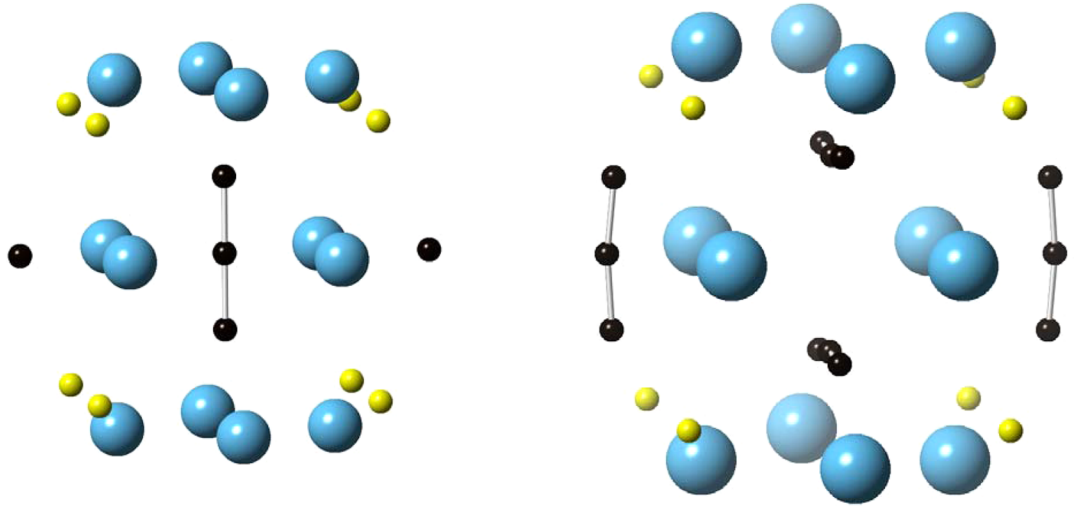

Figure 2. Coordination environment of the allenylide anions in $Ca_{12}InC_{13-x}$ (left) and $Ba_{12}InC_{18}H_4$ (right). Alkaline-earth atoms are blue, and carbon atoms are black; atoms in the 8c site (carbon or hydrogen) are yellow.

dx.doi.org/10.1021/ic502315m | Inorg. Chem. 2015, 54, 914−921

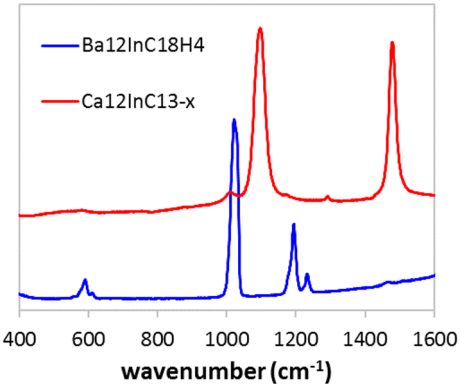

Figure 3. Raman spectra for $Ca_{12}InC_{13-x}$ and $Ba_{12}InC_{18}H_4$.

1480 cm^{-1}; weaker overtone and combination bands were observed at higher wavenumbers (not shown; $2\nu_{sym} \approx 2180$ cm^{-1}, $\nu_{sym} + \nu_{asym} \approx 2550$ cm^{-1}; $2\nu_{asym} \approx 2940$ cm^{-1}). These data are very similar to those reported for $Ca_3C_3Cl_2$, which also contains the C_3^{4-} anion surrounded by calcium cations and had Raman peaks at $\nu_{sym} = 1159$ cm^{-1} and $\nu_{asym} = 1660$ cm^{-1}.[33] The allenylide stretching modes are shifted to lower wavenumbers for $Ba_{12}InC_{18}H_4$ ($\nu_{sym} = 1020$ cm^{-1} and $\nu_{asym} = 1197$ and 1234 cm^{-1}); a bending mode is also seen ($\delta = 593$ cm^{-1}). This is comparable to the C_3^{4-} bending mode observed for $Ca_{11}Sn_3C_8$ ($\delta = 589$ cm^{-1}).[2] No corresponding peak is seen for $Ca_{12}InC_{13-x}$; the higher site symmetry of the C_3^{4-} anions in this structure may make this mode Raman inactive. The energies of the stretching modes of the allenylide anion are likely correlated to the electronegativity of the surrounding cations. Raman spectra reported for Mg_2C_3 show a band at $\nu_{sym} = 1213$ cm^{-1} and a calculated but not observed $\nu_{asym} = 1700$ cm^{-1}. These modes shift to lower energy as the C_3^{4-} anion is surrounded by calcium ($Ca_{12}InC_{13-x}$) and further shift for the barium phase $Ba_{12}InC_{18}H_4$ (ν_{sym} changing from 1213 to 1100 cm^{-1} to 1020 cm^{-1}, respectively). This is similar to what is reported for acetylide anion stretches in the alkaline-earth acetylides, which show the ν_{sym} mode shifting from 1860 cm^{-1} (CaC_2) to 1852 cm^{-1} (SrC_2) to 1831 cm^{-1} (BaC_2).[28]

Electronic Structure. While both $Ca_{12}InC_{13-x}$ and $Ba_{12}InC_{18}H_4$ contain recognizable cations and anions that have commonly accepted formal charges, attempts to derive a charge-balanced state results in a required charge of 4+ for indium $[(Ca^{2+})_{12}(In^{4+})(C_3^{4-})_3(C^{4-})_4$ and $(Ba^{2+})_{12}(In^{4+})(C_3^{4-})_6(H^-)_4]$. These stoichiometries could also be balanced by inferring the presence of In^{3+} and a delocalized hole, which would be in agreement with the presence of a band gap above the Fermi level (vide infra). However, the indium sites are surrounded by calcium cations and not likely to be formally cationic themselves. Thus, the structures cannot possibly be stabilized by charge-balancing. They appear to be aiming instead for similar stabilizing valence electron counts; while the barium phase has twice as many allenylide anions, the substitution of C^{4-} for H^- in $Ca_{12}InC_{13-x}$ allows for both compounds to have identical total formal charges on the anions. The calculated density of states (DOS) data for the two title phases are shown in Figure 4. Both phases have a nonzero DOS at the Fermi level and are therefore metallic. In $Ba_{12}InC_{18}H_4$, the states near E_F are derived from contributions from the carbide anions and their associated barium coordination sphere (which produce bands at and just below the Fermi level) and the indium orbitals (which produce bands at and just above

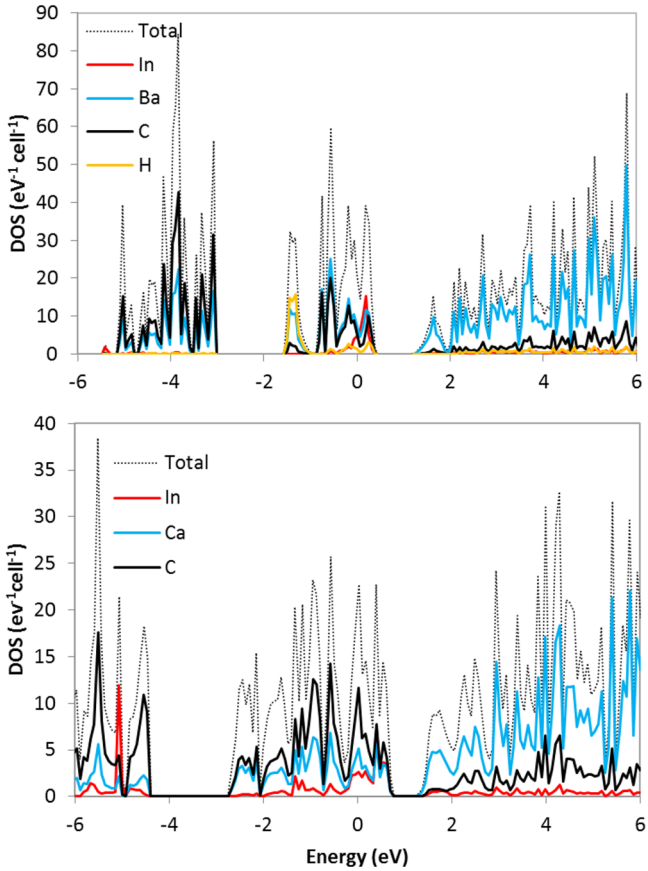

Figure 4. Calculated electronic DOS for $Ca_{12}InC_{13}$ (bottom) and $Ba_{12}InC_{18}H_4$ (top). The Fermi level is set at 0 eV.

E_F). The hydrogen-derived states are, for the most part, localized in a narrow band at around −1.5 eV below E_F, indicating that they are largely anionic.

The DOS for $Ca_{12}InC_{13}$ was calculated using a model structure with full occupancy of all sites; the data show some similarities to that of the barium compound (including a nonzero DOS at E_F and a band gap at around 1 eV above E_F) but some significant differences. There are fewer states at E_F for the calcium phase (11 states/eV/cell vs 21 states/eV/cell for $Ba_{12}InC_{18}H_4$), indicating that while the calcium compound is metallic, it is a poorer metal than the barium phase. The states at the Fermi level are largely derived from carbon orbitals, with smaller contributions from calcium and indium. The Fermi level cuts through a sharp peak in the DOS, which is right above a pseudogap. This might be the driving force for the vacancies on the 8c carbide site; fewer electrons may position E_F in the pseudogap, stabilizing the structure. Similar stabilizing effects of vacancies have been postulated for $LaZn_{0.67}As_2$ and $La_{21-d}Mn_8Te_7C_{12}$.[34,35]

More specific contributions to the DOS near the Fermi level and corresponding COHP data for $Ca_{12}InC_{13}$ are shown in Figure 5. The dominant states at E_F are derived from indium p orbitals and surrounding calcium states and from the p orbitals of the C^{4-} anion (C3 carbon on the 8c site) and associated calcium states. The COHP calculations indicate that the Ca−In and Ca−C3 interactions are strongly bonding at E_F. States from the allenylide anion are predominantly located well below the Fermi level (showing well-stabilized C−C bonding interactions at −4 to −7 eV and antibonding interactions above 2 eV), although the p orbitals of the terminal carbon atoms (C2) of

dx.doi.org/10.1021/ic502315m | Inorg. Chem. 2015, 54, 914−921

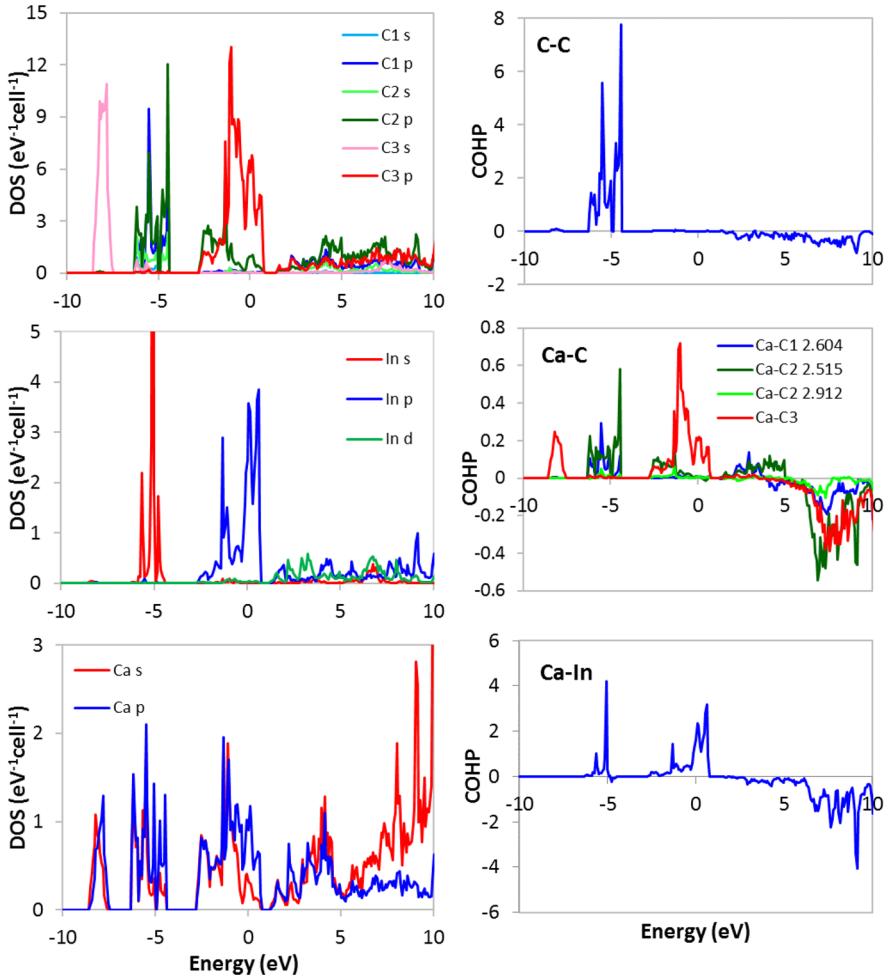

Figure 5. Partial DOS (left column) for specified atomic orbitals and COHP data (right column) for interactions between specified atoms in $Ca_{12}InC_{13}$. The Fermi level is set at 0 eV.

this group do make a small (C−C nonbonding) contribution to states at E_F.

Similar DOS and COHP data for $Ba_{12}InC_{18}H_4$ are shown in Figure 6. As was the case with the calcium compound, indium p orbitals contribute to a very narrow band at the Fermi level; these orbitals have a bonding interaction with surrounding barium ions. The other dominant contributions at E_F are from the p orbitals of the terminal carbon atoms (C2) of the allenylide unit. These states are strongly bonding to surrounding barium ions but are nonbonding to the center carbon of the C_4^{3-} anion. The COHP for the C−C interactions of these anions in $Ba_{12}InC_{18}H_4$ looks very similar to that of the allenylides in $Ca_{12}InC_{13}$: strong C−C bonding interactions below −4 eV\ and antibonding interactions well above E_F. The strength of the C−C double bonds and the large number of C_3^{4-} ions in the unit cell lead to a large integrated COHP of 13.54 eV/cell for these bonds (see Table S3 in the SI). While there are a small number of hydride states at the Fermi level, they are largely nonbonding; most of the hydride states are instead located 1.5 eV below E_F. This hydride band is higher in energy than is typically seen for calcium-based hydrides such as $Ca_{54}In_{13}B_{4-x}H_{23+x}$, $LiCa_2C_3H$, and $LiCa_3As_2H$, all of which have their hydride states 4 eV below the Fermi level.[11,13,14] This may reflect the longer distance between the H^- anion and surrounding Ba^{2+} cations in $Ba_{12}InC_{18}H_4$, which would lead to a weaker interaction. A very small integrated COHP value of 0.37 eV/cell for the Ba−H interaction confirms the weak nature of the bonding (see Table S3 in the SI).

The conduction electrons in $Ca_{12}InC_{13-x}$ and $Ba_{12}InC_{18}H_4$ therefore travel predominantly through the $In@AE_{12}$ clusters. For the calcium compound, states from the C^{4-} anions also contribute to the metallic behavior. The C_3^{4-} allenylide anion bands are not located near the Fermi level and do not participate in electron transport. This is not the case for $Ba_{12}InC_{18}H_4$; the allenylide anions have significant numbers of states at E_F (bonding Ba−C interactions) and may contribute to the metallic behavior of this compound.

CONCLUSIONS

Alkaline-earth-rich melts are excellent solvents for carbon, allowing for the formation and crystal growth of new complex carbides. Flux reactions of carbon in Ca/Li and Ba/Li have enabled the formation of many new phases containing the allenylide anion (C_3^{4-}), which has rarely been seen otherwise. Raman spectroscopy and DOS calculations indicate that these species are largely anionic, although they are building blocks of metallic compounds. Solid-state NMR spectroscopy will be useful in further exploring the nature of these carbide anions.

dx.doi.org/10.1021/ic502315m | Inorg. Chem. 2015, 54, 914−921

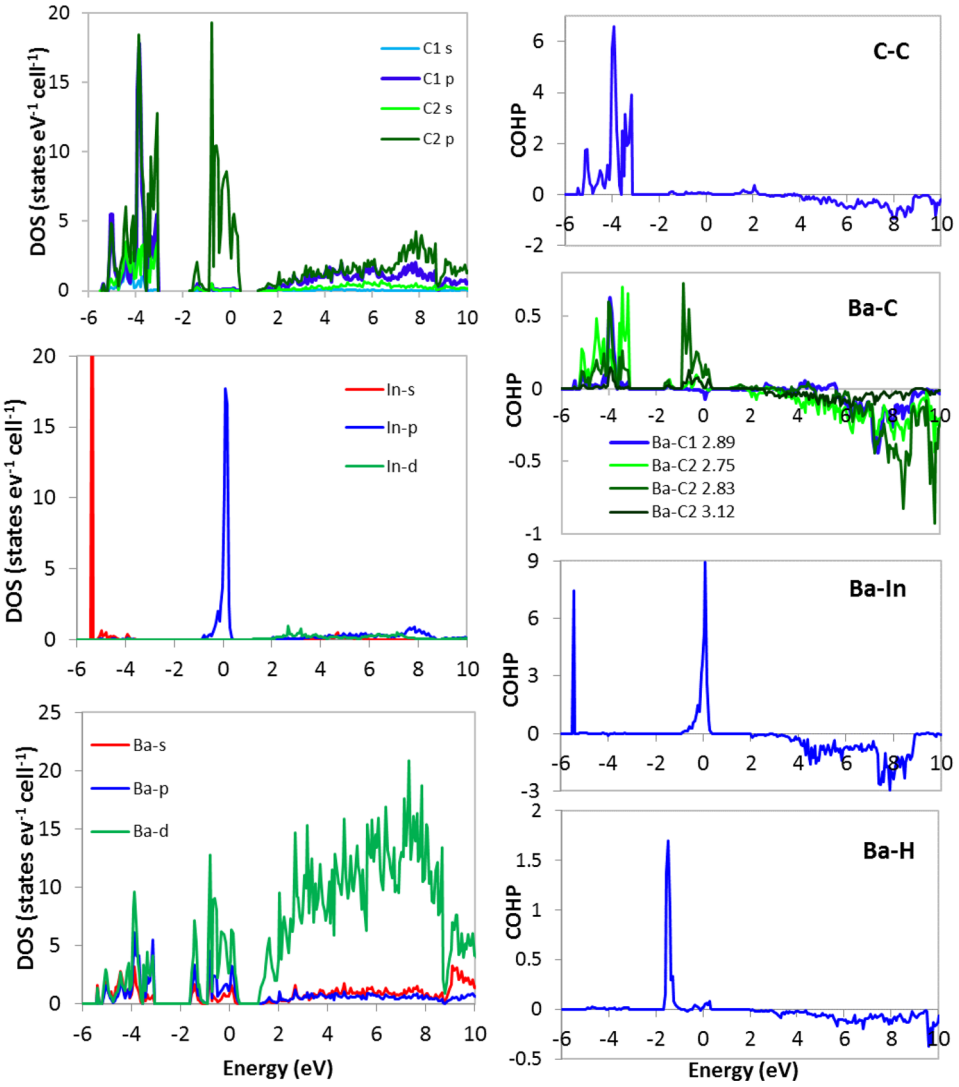

Figure 6. Partial DOS (left column) for specified atomic orbitals and COHP data (right column) for interactions between specified atoms in $Ba_{12}InC_{18}H_4$. The Fermi level is set at 0 eV.

■ ASSOCIATED CONTENT

Supporting Information

Tables of crystallographic data for the $Ca_{12}InC_{13-x}H_x$ refinement model and of integrated COHP values for $Ba_{12}InC_{18}H_4$, mass spectra from hydrolysis reactions of $Ca_{12}InC_{13-x}$ and $Ba_{12}InC_{18}H_4$, and crystallographic data for both phases in CIF format. This material is available free of charge via the Internet at http://pubs.acs.org.

■ AUTHOR INFORMATION

Corresponding Author

*E-mail: latturne@chem.fsu.edu. Phone: 850-644-4074. Fax: 850-644-8281.

Notes

The authors declare no competing financial interest.

■ ACKNOWLEDGMENTS

This research was supported by funding from the National Science Foundation (Division of Materials Research) through Grant DMR-11-06150 and by the FSU Department of Chemistry and Biochemistry. This research made use of the scanning electron microscope facilities of the FSU Physics Department.

■ REFERENCES

(1) Kauzlarich, S. M. *Chemistry, structure, and bonding of Zintl phases and ions*; VCH Publishers, Inc.: New York, 1996.

(2) Blankenship, T. V.; Lita, A.; Latturner, S. E. *Inorg. Chem.* **2012**, *51*, 13345−13350.

(3) Villars, P.; Calvert, L. D. *Pearson's Handbook—Crystallographic Data for Intermetallic Phases*; ASM International: Materials Park, OH, 1998.

(4) Sevov, S. C.; Corbett, J. D. *Inorg. Chem.* **1991**, *30*, 4875.

(5) Li, B.; Corbett, J. D. *Inorg. Chem.* **2003**, *42*, 8768−8772.

(6) Li, B.; Corbett, J. D. *J. Am. Chem. Soc.* **2005**, *127*, 926−932.

(7) Henning, R. W.; Leon-Escamilla, E. A.; Zhao, J. T.; Corbett, J. D. *Inorg. Chem.* **1997**, *36*, 1282−1285.

(8) Huang, B.; Corbett, J. D. *Inorg. Chem.* **1998**, *37*, 1892−1899.

(9) Kanatzidis, M. G.; Pöttgen, R.; Jeitschko, W. *Angew. Chem., Int. Ed.* **2005**, *44*, 6996−6702.

(10) Massalski, T. B.; Okamoto, H. *Binary Alloy Phase Diagrams*, 2nd ed.; ASM International: Materials Park, OH, 1990.

(11) Lang, D. A.; Zaikina, J. V.; Lovingood, D. D.; Gedris, T. E.; Latturner, S. E. *J. Am. Chem. Soc.* **2010**, *132*, 17532−17530.

(12) Lang, D. A.; Latturner, S. E. *Eur. J. Inorg. Chem.* **2011**, *26*, 4006−4011.
(13) Blankenship, T. V.; Wang, X.; Hoffmann, C.; Latturner, S. E. *Inorg. Chem.* **2014**, *53* (19), 10620−10626.
(14) Blankenship, T. V.; Chen, B.; Latturner, S. E. *Chem. Mater.* **2014**, *26*, 3202−3208.
(15) *SAINT*, version 6.02a; Bruker AXS Inc.: Madison WI, 2000.
(16) Sheldrick, G. M. *SHELXTL NT/2000*, version 6.1; Bruker AXS, Inc.: Madison, WI, 2000.
(17) Spek, A. L. *Acta Crystallogr.* **2009**, *D65*, 148−155.
(18) (a) Jepsen, O.; Burkhardt, A.; Andersen, O. K. *Program TB-LMTO-ASA*, version 4.7; Max-Planck-Institut für Festkörperforschung: Stuttgart, Germany, 2000. (b) Blöchl, P. E.; Jepsen, O.; Andersen, O. K. *Phys. Rev. B* **1994**, *49*, 16223−16233.
(19) (a) Fornasini, M. L. *Acta Crystallogr., Sect. C* **1987**, *43*, 613−616. (b) Marsh, R. E.; Slagle, K. M. *Acta Crystallogr., Sect. C* **1988**, *44*, 395−396.
(20) Mao, J. G.; Goodey, J.; Guloy, A. M. *Inorg. Chem.* **2004**, *43*, 282−289.
(21) Wendorff, M.; Röhr, C. *Z. Naturforsch. B* **2004**, *59*, 619−628.
(22) Wendorff, M.; Scherer, H.; Röhr, C. *Z. Anorg. Allg. Chem.* **2010**, *636*, 1038−1044.
(23) Wendorff, M.; Röhr, C. *Z. Naturforsch. B* **2008**, *63*, 804−818.
(24) Snyder, G. J.; Borrmann, H.; Simon, A. *Z. Kristallogr.* **1994**, *209*, 458.
(25) Reckeweg, O.; Molstad, J. C.; Levy, S.; DiSalvo, F. J. *Z. Naturforsch.* **2007**, *62b*, 23−27.
(26) Bronger, W.; Kniep, R.; Kohout, M. *Z. Anorg. Allg. Chem.* **2005**, *631*, 265−271.
(27) Kurakevych, O. O.; Strobel, T. A.; Kim, D. Y.; Cody, G. D. *Angew. Chem., Int. Ed.* **2013**, *52*, 8930−8933.
(28) Ruschewitz, U. *Coord. Chem. Rev.* **2003**, *244*, 115−136.
(29) Czekalla, R.; Jeitschko, W.; Hoffmann, R. D.; Rabeneck, H. *Z. Naturforsch. B* **1996**, *51*, 646−654..
(30) Pöttgen, R.; Jeitschko, W. *Inorg. Chem.* **1991**, *30*, 427−431.
(31) Pöttgen, R.; Wachtmann, K. H.; Jeitschko, W.; Lang, A.; Ebel, T. *Z. Naturforsch. B* **1997**, *52*, 231−236.
(32) (a) Fjellvag, H.; Karen, P. *Inorg. Chem.* **1992**, *31*, 3260−3263. (b) Karen, P.; Fjellvag, H. *J. Alloys Compd.* **1992**, *178*, 285−295. (c) Disch, S.; Cheetham, A. K.; Ruschewitz, U. *Inorg. Chem.* **2008**, *47*, 969−973.
(33) (a) Hoffmann, R.; Meyer, H. J. *Z. Anorg. Allg. Chem.* **1992**, *607*, 57−71. (b) Meyer, H. J. *Z. Anorg. Allg. Chem.* **1991**, *593*, 185−192.
(34) Stoyko, S. S.; Mar, A. *J. Solid State Chem.* **2011**, *184*, 2360−2367.
(35) Zaikina, J. V.; Schellenberg, I.; Benbow, E. M.; Pöttgen, R.; Latturner, S. E. *Chem. Mater.* **2011**, *23*, 1768−1778.